Journal of Clinical and Translational Hepatology **2026** vol. 14(4) | 367–382
DOI: 10.14218/JCTH.2025.00616

Original Article

A Multi-omics Investigation Identifies TACC3 as a Driver of Immunosuppression in Intrahepatic Cholangiocarcinoma via Activation of the STAT3-PD-L1 Axis

Hao Wang[1#], Zhiquan Xu[1#], Ziqi Zhang[1], Yan You[1], Ranning Xu[1], Hongli Chen[2], Hongshuai Cui[3], Xiaoyong Luo[4*] and Rui Liao[1*]

[1]Department of Hepatobiliary Surgery, the First Affiliated Hospital of Chongqing Medical University, Chongqing, China; [2]Office of the Dean, Chongqing Nanchuan District Maternal and Child Health Hospital, Chongqing, China; [3]Department of Gastrointestinal Surgery, Qingdao Central Hospital, University of Health and Rehabilitation Sciences, Qingdao, Shandong, China; [4]Department of Gastrointestinal and Thoracic Surgery, Chongqing Jiulongpo People's Hospital, Chongqing, China

Received: November 17, 2025 | **Revised:** January 13, 2026 | **Accepted:** March 17, 2026 | **Published online:** April 10, 2026

Abstract

Background and Aims: The immunosuppressive tumor microenvironment (TME) limits immunotherapy efficacy in intrahepatic cholangiocarcinoma (ICC). Understanding the molecular drivers of this TME is essential for developing new therapies. This study aimed to identify novel oncogenes that modulate the immune landscape of ICC using a multi-omics approach. ***Methods:*** We integrated transcriptomic and proteomic data from our ICC cohorts with public datasets (TCGA-CHOL, GSE107943, OEP002768) to identify genes co-upregulated with PD-L1 (CD274). Single-cell RNA sequencing (scRNA-seq) was used to analyze cell-type-specific expression and intercellular communication. Clinical significance was validated through tissue microarrays and multiplex immunofluorescence in an independent ICC cohort. ***Results:*** Multi-omics screening identified TACC3 as a key candidate in ICC. Elevated TACC3 expression in ICC tissues correlated with poor prognosis and promoted tumor cell proliferation and migration. TACC3 activated the STAT3 pathway, increasing PD-L1 transcription. scRNA-seq showed TACC3/PD-L1 interaction in malignant epithelial cells, with PD-L1 co-expressed with FOXP3 in regulatory T cells (Tregs). Cell–cell communication analysis predicted strong interactions between malignant cells and Tregs. TACC3 knockdown reduced PD-L1 expression and inhibited STAT3 and AKT phosphorylation. Clinical validation confirmed co-expression of TACC3, PD-L1, and FOXP3, with high TACC3 levels linked to worse clinicopathological features and shorter progression-free survival. ***Conclusions:*** Our study defines a TACC3-STAT3-PD-L1 axis driving immunosuppression in ICC. TACC3 fosters an immunosuppressive TME by upregulating PD-L1 and is associated with a Treg-rich contexture, suggesting that TACC3 may serve as a potential therapeutic target to overcome ICC immunosuppression.

Citation of this article: Wang H, Xu Z, Zhang Z, You Y, Xu R, Chen H, *et al*. A Multi-omics Investigation Identifies TACC3 as a Driver of Immunosuppression in Intrahepatic Cholangiocarcinoma via Activation of the STAT3-PD-L1 Axis. J Clin Transl Hepatol 2026;14(4):367–382. doi: 10.14218/JCTH.2025.00616.

Introduction

Intrahepatic cholangiocarcinoma (ICC) is a highly aggressive malignancy arising from the biliary epithelium, characterized by a high incidence of late diagnosis, limited treatment options, and a dismal prognosis.[1–3] While immunotherapy, particularly immune checkpoint inhibitors targeting the PD-1/PD-L1 axis, has revolutionized the treatment of many solid tumors, its efficacy in ICC remains limited and heterogeneous.[4,5] A primary factor contributing to this resistance is the profoundly immunosuppressive tumor microenvironment (TME), which is often enriched with regulatory T cells (Tregs) and exhibits upregulation of PD-L1.[6] However, the key molecular drivers that initiate and sustain this immunosuppressive landscape in ICC are not fully elucidated, hindering the development of effective therapeutic strategies to reprogram the TME.

Current evidence suggests that oncogenic signaling pathways play a crucial role in modulating the immune TME.[7,8] However, the upstream oncogenes responsible for the specific upregulation of PD-L1 in ICC remain poorly understood. This gap is particularly important, as understanding the precise molecular drivers of PD-L1 upregulation is crucial for developing more effective therapeutic strategies. The STAT3 pathway, in particular, is a well-known mediator of tumorigenesis and immune evasion in various cancers, including ICC.[9] STAT3 activation can directly transcriptionally upregulate PD-L1 and promote the recruitment and function of immunosuppressive cells.[10] Despite this knowledge, the upstream regulators that orchestrate STAT3 activation and its interplay with PD-L1 in the context of ICC-specific immunosuppression

Keywords: Intrahepatic cholangiocarcinoma; TACC3; STAT3; PD-L1; Tumor microenvironment; Immunosuppression; Multi-omics; Prognosis.

[#]Contributed equally to this work.

[*]**Correspondence to:** Xiaoyong Luo, Department of Gastrointestinal and Thoracic Surgery, Chongqing Jiulongpo People's Hospital, Chongqing 400050, China. ORCID: https://orcid.org/0009-0008-8075-609X, Tex: +86-23-68859068, Fax: +86-23-68859066, E-mail: 19402704@qq.com; Rui Liao, Department of Hepatobiliary Surgery, the First Affiliated Hospital of Chongqing Medical University, Chongqing 400016, China. ORCID: https://orcid.org/0000-0002-2792, Tex: +86-23-86528009, Fax: +86-23-89038154, E-mail: liaorui99@163.com.

remain an area of active investigation. A systematic, multi-omics approach is needed to identify such key upstream oncogenes that functionally link tumor-intrinsic signaling with the establishment of an immunosuppressive TME.

In this study, we conducted an integrated multi-omics analysis to identify novel drivers that are co-upregulated with PD-L1 and associated with poor outcomes in ICC. Through this screening, we identified transforming acidic coiled-coil containing protein 3 (TACC3), a centrosome- and mitotic spindle-associated protein implicated in cell cycle progression, as a top candidate.[11] Although TACC3 dysregulation has been observed in several cancers, its precise role, particularly in modulating the immune TME of ICC, is entirely unknown.

Therefore, the aims of this study were to: 1) validate TACC3 as a key prognostic oncogene in ICC; 2) elucidate the mechanistic link between TACC3 and PD-L1 regulation; 3) investigate the role of TACC3 in shaping the immunosuppressive TME using single-cell transcriptomics and cellular assays; and 4) determine the clinical relevance of the TACC3-associated signaling axis in a well-annotated patient cohort. Our work sought to define a novel pathogenic pathway in ICC and identify TACC3 as a potential therapeutic target for overcoming immunosuppression.

Methods

Patient samples

This study utilized two independent cohorts from The First Affiliated Hospital of Chongqing Medical University. The discovery cohort consisted of 18 fresh-frozen ICC samples, which were used for transcriptomic and proteomic profiling. The validation cohort comprised a tissue microarray (TMA) containing 90 ICC cases with detailed clinicopathological data, including 87 matched tumor and peritumoral tissues and 3 cases with tumor tissue only.

Multi-omics data acquisition and immunohistochemistry (IHC)

For the in-house cohort, RNA sequencing was performed on an Illumina NovaSeq 6000 platform.[12] Proteomic profiling was conducted using liquid chromatography-tandem mass spectrometry. PD-L1 IHC was performed on formalin-fixed paraffin-embedded sections using the Dako 22C3 pharmDx assay.[13] The Tumor Proportion Score (TPS) was employed for assessment, defined as the percentage of viable tumor cells exhibiting partial or complete linear membrane staining at any intensity. Using a clinically validated cut-off value of TPS ≥ 1%, samples were categorized as PD-L1 positive (n = 7) or PD-L1 negative (n = 11). Public datasets, including TCGA-CHOL, GSE107943, and OEP002768, were downloaded for independent validation. Single-cell RNA sequencing (scRNA-seq) data were integrated from GSE181878, GSE138709, and GSE151530. Bioinformatic analyses, including differential expression analysis, Gene Set Enrichment Analysis (GSEA), and Gene Ontology (GO)/Kyoto Encyclopedia of Genes and Genomes (KEGG) enrichment, were performed using R packages DESeq2 and clusterProfiler.

Cell lines and culture conditions

Human ICC cell lines (HUCCT1, HCCC9810, RBE) and the human intrahepatic biliary epithelial cell line HIBEpiC were purchased from Cellverse Co., Ltd (Shanghai, China). All cell lines were cultured in RPMI-1640 medium supplemented with 10% fetal bovine serum (FBS, Gibco) at 37 °C in a 5% CO_2 incubator. Cell lines were authenticated by STR profiling and tested negative for mycoplasma contamination.

Plasmid construction and TACC3 knockdown

TACC3 knockdown was achieved using plasmids synthesized by Tsingke Biotechnology Co., Ltd (Beijing, China). The plasmids containing short hairpin RNA targeting TACC3 and a non-targeting control were transfected into ICC cells using Lipofectamine 3000 (Invitrogen) according to the manufacturer's protocol.[14] Knockdown efficiency was verified by Western blotting 48–72 h post-transfection.

Western blot analysis

Cells were lysed using RIPA lysis buffer containing protease and phosphatase inhibitors. Proteins were separated by SDS-PAGE and transferred to PVDF membranes. Membranes were blocked and incubated overnight at 4 °C with primary antibodies against TACC3 (Huabio, Hangzhou, China, Clone SN73-05), PD-L1 (Cell Signaling Technology, 13684), STAT3 (CST, 12640), p-STAT3 (Tyr705, CST, 9145), AKT (CST, 4691), p-AKT (Ser473, CST, 4060), and GAPDH (CST, 5174). After incubation with HRP-conjugated secondary antibodies, protein bands were visualized using an enhanced chemiluminescence detection system.[15]

Cell proliferation assay

Cell proliferation was assessed using the CCK-8 kit (Dojindo) according to the manufacturer's instructions. Briefly, 2,000 cells/well were seeded in 96-well plates after transfection. At designated time points, 10 μL of CCK-8 solution was added to each well and incubated for 2 h at 37 °C. The optical density at 450 nm was measured using a microplate reader.[16]

Cell migration assays

For wound healing assays, cells were seeded in 6-well plates and cultured until 90% confluent. A sterile 200 μL pipette tip was used to create a straight scratch. Cell migration was monitored and photographed at 0, 24, and 48 h. For Transwell assays, 5×10^4 cells in serum-free medium were placed into the upper chamber of a Transwell insert (Corning), while medium containing 10% FBS was added to the lower chamber as a chemoattractant. After 24 h of incubation, cells that migrated to the lower membrane surface were fixed, stained, and counted under a microscope.[17]

scRNA-seq analysis

scRNA-seq data from multiple cohorts (GSE181878, GSE138709, GSE151530) were integrated and analyzed using the Seurat and Harmony packages in R. Cell types were annotated based on canonical marker genes. Cell–cell communication analysis was performed using CellChat to infer ligand-receptor interactions between different cell populations.[18]

TMA and multiplex immunofluorescence (mIF)

The TMA containing 90 ICC cases was constructed from formalin-fixed paraffin-embedded tissues. Multiplex immunofluorescence was performed using the Opal™ 7-Color Manual IHC Kit (Akoya Biosciences) with antibodies against TACC3 (Huabio), CD274 (PD-L1), and FOXP3. Slides were scanned using a Vectra Polaris imaging system and quantitatively analyzed using QuPath software.[19]

Statistical analysis

All statistical analyses were performed using R software (v4.5.1) or GraphPad Prism (v10.6.1). Data are presented as mean ± standard deviation from at least three independent experiments. Group comparisons were analyzed using Student's t-test (for two groups) or one-way ANOVA (for multiple

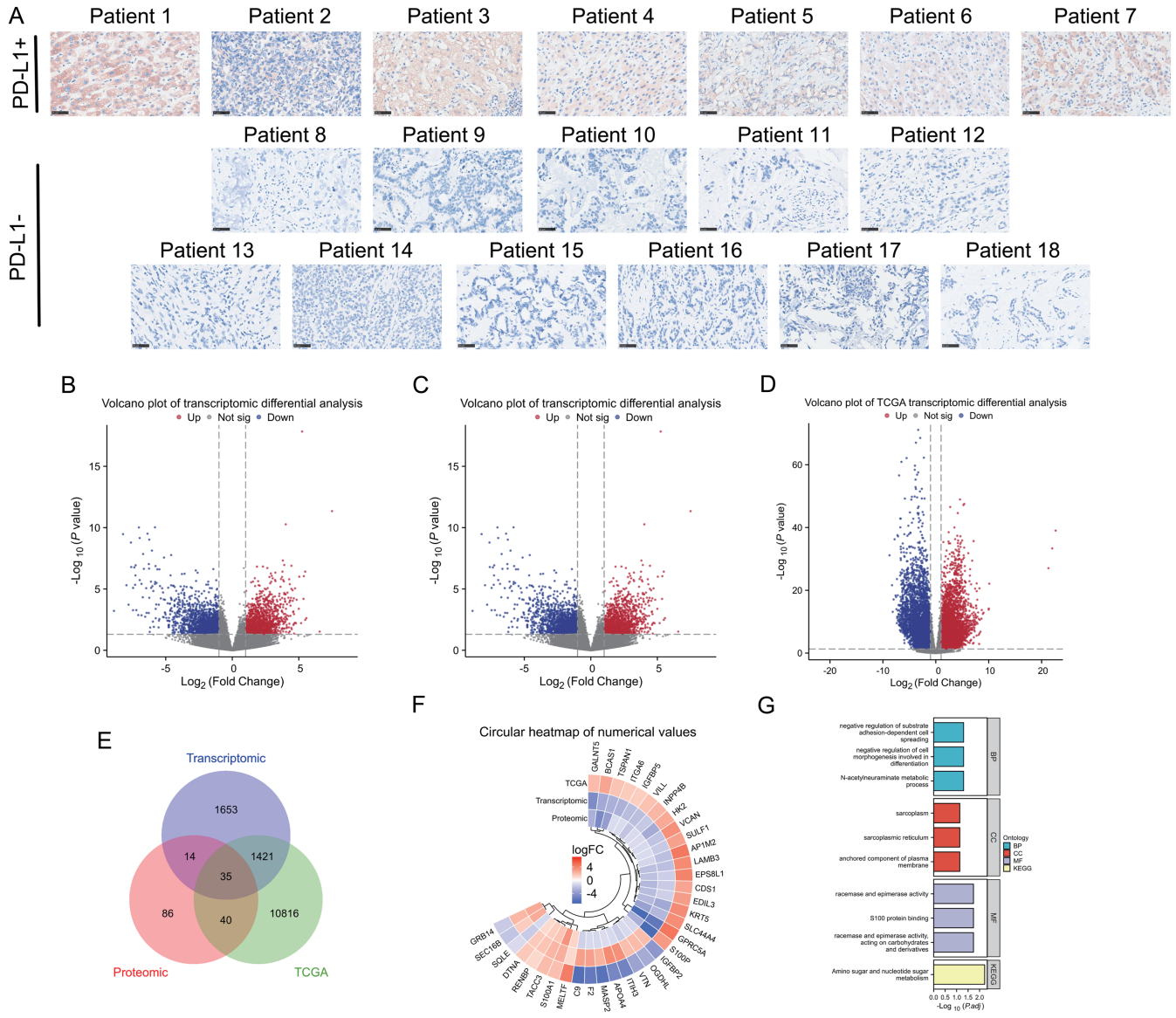

Fig. 1. Multi-omics screening for candidate genes in ICC. (A) Representative IHC images of PD-L1 expression in ICC tissues, categorized into PD-L1-positive and -negative groups based on the TPS (n = 7 vs. n = 11). (B–D) Volcano plots depicting DEGs. (B) Transcriptomic DEGs between PD-L1-positive and -negative ICC tissues (1,517 upregulated, 1,606 downregulated). (C) Proteomic DEGs between the same groups (115 upregulated, 65 downregulated). (D) DEGs between ICC tumors and adjacent normal tissues from the TCGA-CHOL cohort (7,547 upregulated, 4,765 downregulated). (E) Venn diagram illustrating the intersection of DEGs from the transcriptome, proteome, and tumor-associated genes from TCGA. (F) Chord plot visualizing the consistent LogFC expression patterns of the 35 candidate genes across the transcriptomic and proteomic datasets, highlighting genes with concordant upregulation or downregulation. (G) GO and KEGG pathway bar charts for the final shortlisted candidate genes. ICC, intrahepatic cholangiocarcinoma; IHC, immunohistochemistry; TPS, Tumor Proportion Score; DEGs, differentially expressed genes; TCGA-CHOL, The Cancer Genome Atlas Cholangiocarcinoma; LogFC, log2 fold change; GO, Gene Ontology; KEGG, Kyoto Encyclopedia of Genes and Genomes.

groups). Correlation analyses were performed using Pearson or Spearman methods. Survival analysis was conducted with Kaplan–Meier curves and log-rank tests. A *P*-value < 0.05 was considered statistically significant.

Results

Multi-omics screening identifies five candidate oncogenes correlated with PD-L1 expression

To identify key regulators of the immune microenvironment in ICC, we began by assessing PD-L1 protein expression in our cohort of clinical ICC samples. Using IHC with the TPS, we stratified the samples into PD-L1-positive (n = 7) and PD-L1-negative (n = 11) groups (Fig. 1A).

Subsequently, we performed transcriptomic and proteomic profiling on these samples to uncover genes associated with PD-L1 expression. Transcriptomic sequencing revealed 1,517 upregulated and 1,606 downregulated differentially expressed genes (DEGs) between the PD-L1-positive and negative groups (Fig. 1B). Parallel proteomic analysis identified 115 upregulated and 65 downregulated proteins (Fig. 1C). To further distill these findings and focus on genes with direct relevance to ICC tumorigenesis, we integrated data

from the TCGA-CHOL cohort. Analysis of TCGA data comparing ICC tumors to adjacent normal tissues identified 7,547 upregulated and 4,765 downregulated DEGs (Fig. 1D).

By taking the intersection of the PD-L1-associated DEGs from our transcriptomic and proteomic datasets with the tumor-associated DEGs from TCGA, we identified 35 core candidate genes that were consistently co-upregulated with PD-L1 and in the tumor context (Fig. 1E). From this pool, we applied a stringent selection process. First, genes were selected based on their LogFC, requiring consistency across datasets with a LogFC threshold of ≥1.5, ensuring robust upregulation of gene expression. Second, we prioritized genes whose biological functions were directly related to tumorigenesis and immune evasion, specifically focusing on those involved in key oncogenic pathways such as cell proliferation and immune modulation. These criteria resulted in five candidate oncogenes—DTNA, RENBP, TACC3, S100A1, and MELTF—which were not only positively correlated with PD-L1 expression but also exhibited pro-tumorigenic characteristics (Fig. 1F).

Finally, to elucidate the potential functional roles of these five shortlisted genes, we performed GO and KEGG pathway enrichment analyses. The GO analysis indicated their significant involvement in key biological processes, including negative regulation of substrate adhesion-dependent cell spreading and negative regulation of cell morphogenesis involved in differentiation. KEGG pathway analysis further suggested their association with amino sugar and nucleotide sugar metabolism (Fig. 1G).

TACC3 is identified as a pivotal oncogene with diagnostic and clinical significance

To prioritize a key driver from the five candidate oncogenes (DTNA, RENBP, TACC3, S100A1, and MELTF), we evaluated their prognostic relevance using the OEP002768 cohort. Overall survival analysis revealed that high expression of three genes—DTNA (P = 0.0034), S100A1 (P = 0.05), and TACC3 (P = 0.004)—was significantly associated with poorer patient survival (Fig. 2A–E). Consistent with their pro-tumorigenic roles, higher expression was associated with poorer prognosis. However, DTNA and S100A1 were excluded due to inconsistencies in their expression patterns or weaker statistical support. Consequently, TACC3 was selected for subsequent investigation due to its strong and significant prognostic value.

We further explored the clinical relevance of TACC3 expression within the same cohort. Elevated TACC3 expression was significantly correlated with aggressive clinicopathological features. Specifically, TACC3 levels were higher in patients with liver cirrhosis (Fig. 2F), advanced TNM stage (Fig. 2G), and lower serum albumin levels (Fig. 2H), suggesting a role in disease progression.

The diagnostic and staging potential of TACC3 was validated using the independent TCGA-CHOL dataset. TACC3 expression demonstrated an exceptional ability to distinguish ICC tumors from normal tissues, with an area under the curve (AUC) of 0.994 (Fig. 2I). Furthermore, it showed a significant albeit moderate capacity to predict advanced T-stage (AUC = 0.611), indicating its association with tumor invasion (Fig. 2J).

To gain mechanistic insight, we performed GO enrichment analysis on TACC3. The results indicated that TACC3 is predominantly involved in critical mitotic processes, including the metaphase/anaphase transition of the cell cycle and the regulation of mitotic sister chromatid separation (Fig. 2K), implicating it in the loss of cell cycle control in ICC.

Finally, to substantiate the initial multi-omics finding that linked TACC3 to immune evasion, we examined its correlation with CD274 (PD-L1) in two independent datasets. Consistent with our hypothesis, TACC3 expression was significantly elevated in tumor tissues (T) compared to adjacent normal tissues (N) in both the TCGA-CHOL and GSE107943 cohorts. Critically, CD274 expression followed the same pattern, showing a strong co-upregulation with TACC3 in tumors (Fig. 2L and M), reinforcing their potential functional association in ICC.

TACC3 expression correlates with PD-L1 and is linked to STAT3-mediated transcriptional regulation

To further validate the relationship between TACC3 and immune checkpoint expression, we assessed the correlation between TACC3 and CD274 (PD-L1) across multiple independent datasets. Consistent positive correlations were observed in the Proteomic cohort (R = 0.528, P = 0.024), the OEP002768 cohort (R = 0.317, P < 0.001), and the GSE107943 dataset (R = 0.357, P = 0.007) (Fig. 3A–C), robustly confirming their co-expression in ICC.

To elucidate the potential signaling pathways through which TACC3 operates, we performed GSEA on the proteomic data, stratified by TACC3 expression. This analysis revealed that high TACC3 expression was positively enriched for pathways including 'Complement Cascade', 'G-protein Coupled Receptor Ligand Binding', and 'Cell–Cell Junction Organization' (Fig. 3D), all of which have previously been implicated in STAT3 activation.[20–22] Conversely, pathways such as 'Cellular Response to Starvation', 'Response of EIF2AK4 (Gcn2) to Amino Acid Deficiency', and 'Foxo-Mediated Transcription of Cell Cycle Genes' were negatively enriched (Fig. 3E), processes known to be inversely correlated with or suppressed by STAT3 signaling.[23–25] This reciprocal enrichment pattern strongly suggested a functional connection between TACC3 and the STAT3 pathway.

Given the central role of STAT3 as a transcription factor and its predicted binding motif, we investigated its direct regulatory potential on CD274. Using the JASPAR database, we identified several high-confidence STAT3 binding sites within the promoter region of the CD274 gene (Fig. 3F and G), positioning STAT3 as a direct transcriptional regulator.

Finally, to consolidate the hypothesis that STAT3 acts as a critical nexus linking TACC3 to PD-L1 upregulation, we performed correlation analyses in all three datasets. In the Proteomic cohort, STAT3 expression showed significant positive correlations with both TACC3 (R = 0.590, P = 0.010) and CD274 (R = 0.541, P = 0.020) (Fig. 3H and I). These correlations were robustly recapitulated in the larger OEP002768 cohort (STAT3–TACC3: R = 0.255, P < 0.001; STAT3–CD274: R = 0.258, P < 0.001; Fig. 3J and K) and the GSE107943 dataset (STAT3–TACC3: R = 0.438, P < 0.001; STAT3–CD274: R = 0.593, P < 0.001; Fig. 3L and M). This consistent, multi-cohort evidence strongly supports the existence of a TACC3–STAT3–PD-L1 regulatory axis in ICC.

PD-L1 (CD274) expression shapes an immunosuppressive microenvironment and is linked to a shared miRNA regulator

To delineate the impact of PD-L1 (encoded by CD274) on the immune landscape of ICC, we performed single-sample GSEA after stratifying samples based on CD274 expression levels. This analysis, conducted across the Proteomic, OEP002768, and GSE107943 datasets, consistently revealed that high CD274 expression was robustly associated with increased infiltration of plasmacytoid dendritic cells (pDCs) and Tregs (Fig. 4A–C).

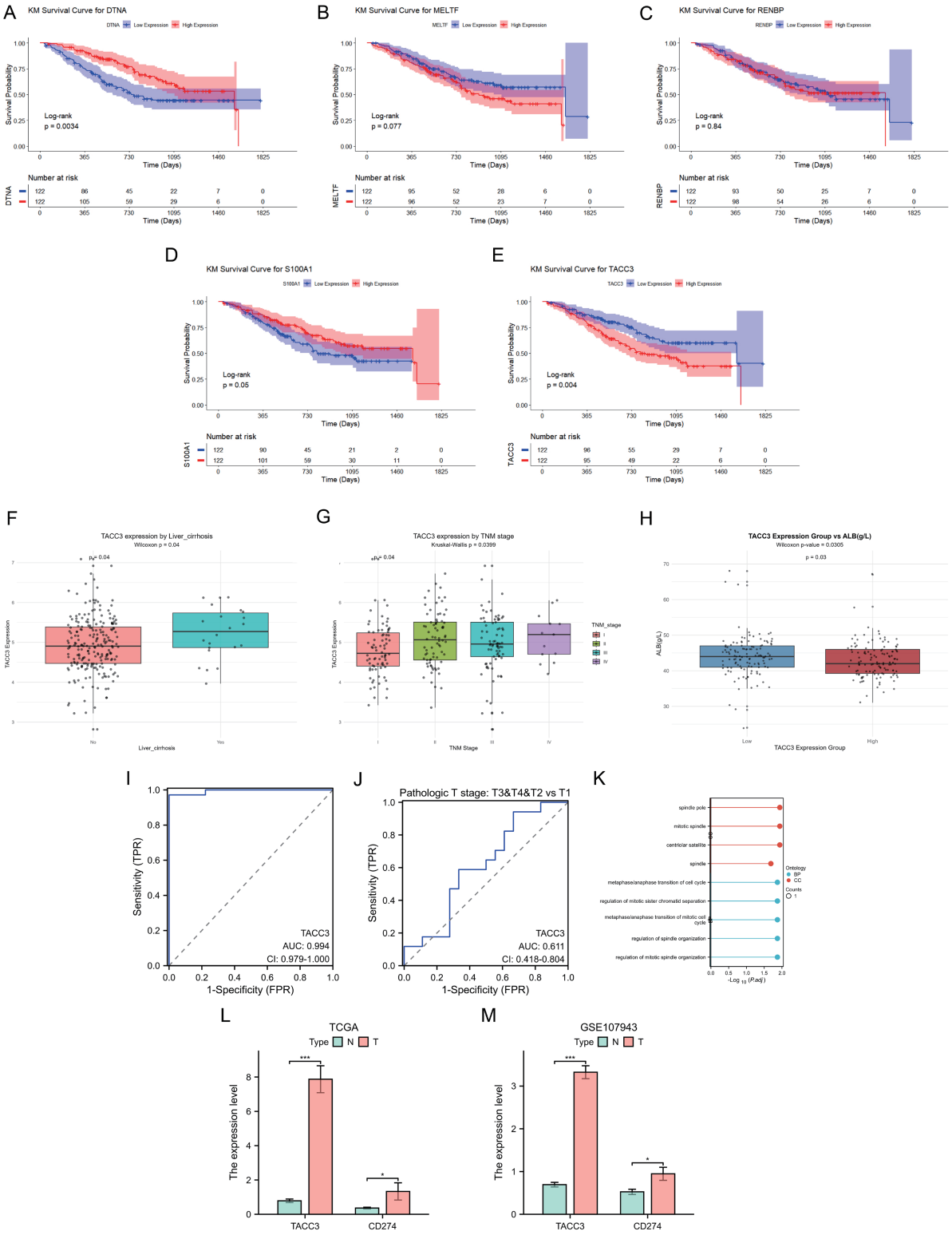

Fig. 2. Clinical correlation and diagnostic value of TACC3 expression in ICC. (A–H) Data from the OEP002768 cohort. (A–E) Kaplan-Meier curves of OS for five candidate genes (DTNA, RENBP, TACC3, S100A1, MELTF). (F) TACC3 expression in patients with and without liver cirrhosis. (G) TACC3 expression across different TNM stages. (H) TACC3 expression in high- and low-ALB groups. (I–M) Data from the TCGA-CHOL cohort. (I) Diagnostic ROC curve of TACC3. (J) ROC curve of TACC3 for T-stage stratification in the TCGA-CHOL cohort. (K) GO functional enrichment analysis results for TACC3. (L, M) Box plots of TACC3 expression in TCGA-CHOL and GSE107943 datasets, respectively. ICC, intrahepatic cholangiocarcinoma; OS, overall survival; TNM, tumor-node-metastasis; ALB, albumin; ROC, receiver operating characteristic; T-stage, tumor stage; TCGA-CHOL, The Cancer Genome Atlas Cholangiocarcinoma; GO, Gene Ontology.

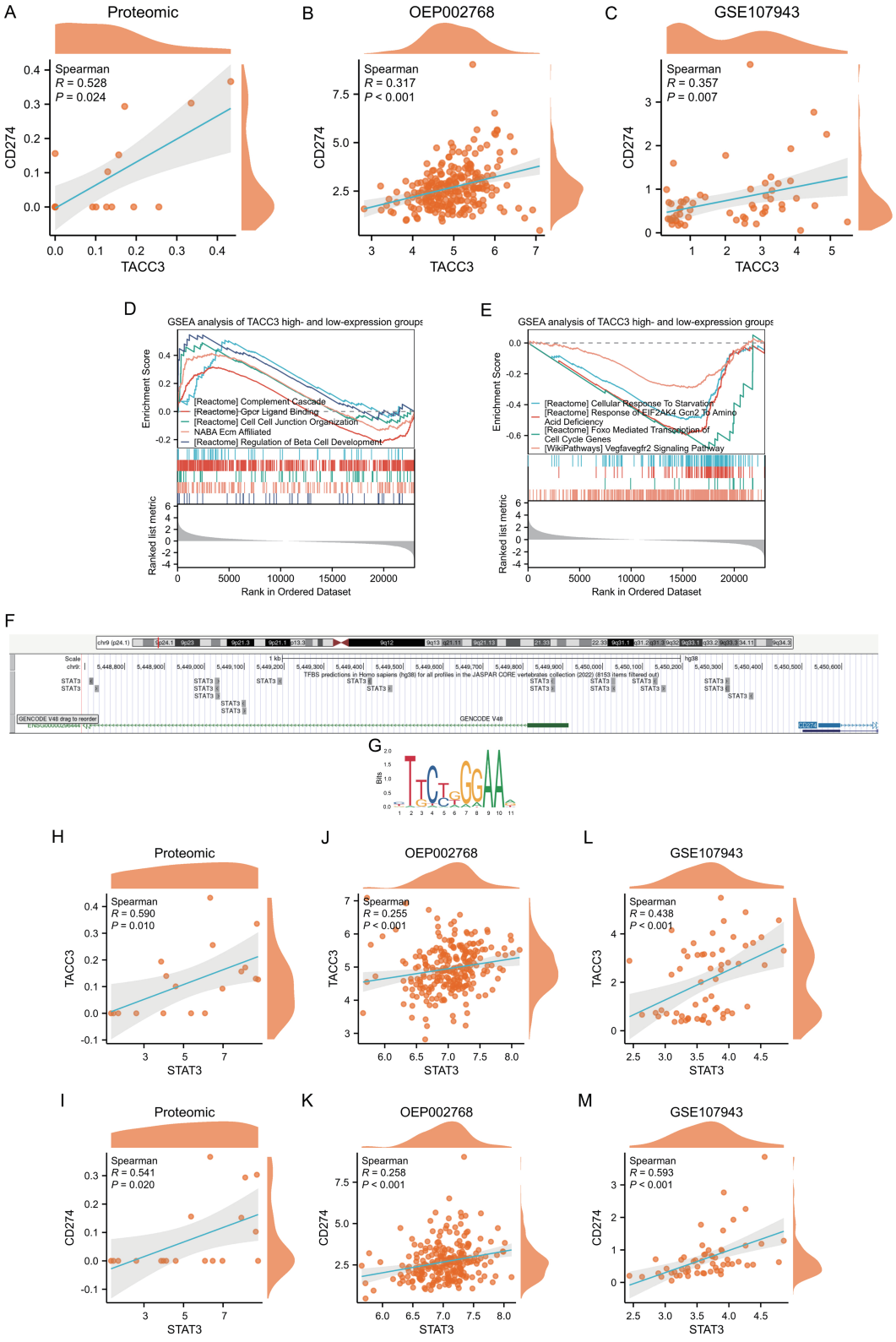

Fig. 3. Correlation analysis of TACC3 and CD274 expression, and assessment of the STAT3 pathway. (A–C) Scatter plots showing TACC3 and PD-L1 (CD274) expression in proteomic, OEP002768, and GSE107943 datasets. (D–F) Pathway and promoter analysis results: (D–E) GSEA plots of proteomic data based on TACC3 expression. (F) *In silico* prediction of STAT3 binding to the CD274 promoter. (G) STAT3 binding motif logo. (H–M) Scatter plots showing the correlation between TACC3 and STAT3, and between PD-L1 (CD274) and STAT3 in proteomic, OEP002768, and GSE107943 datasets. GSEA, Gene Set Enrichment Analysis.

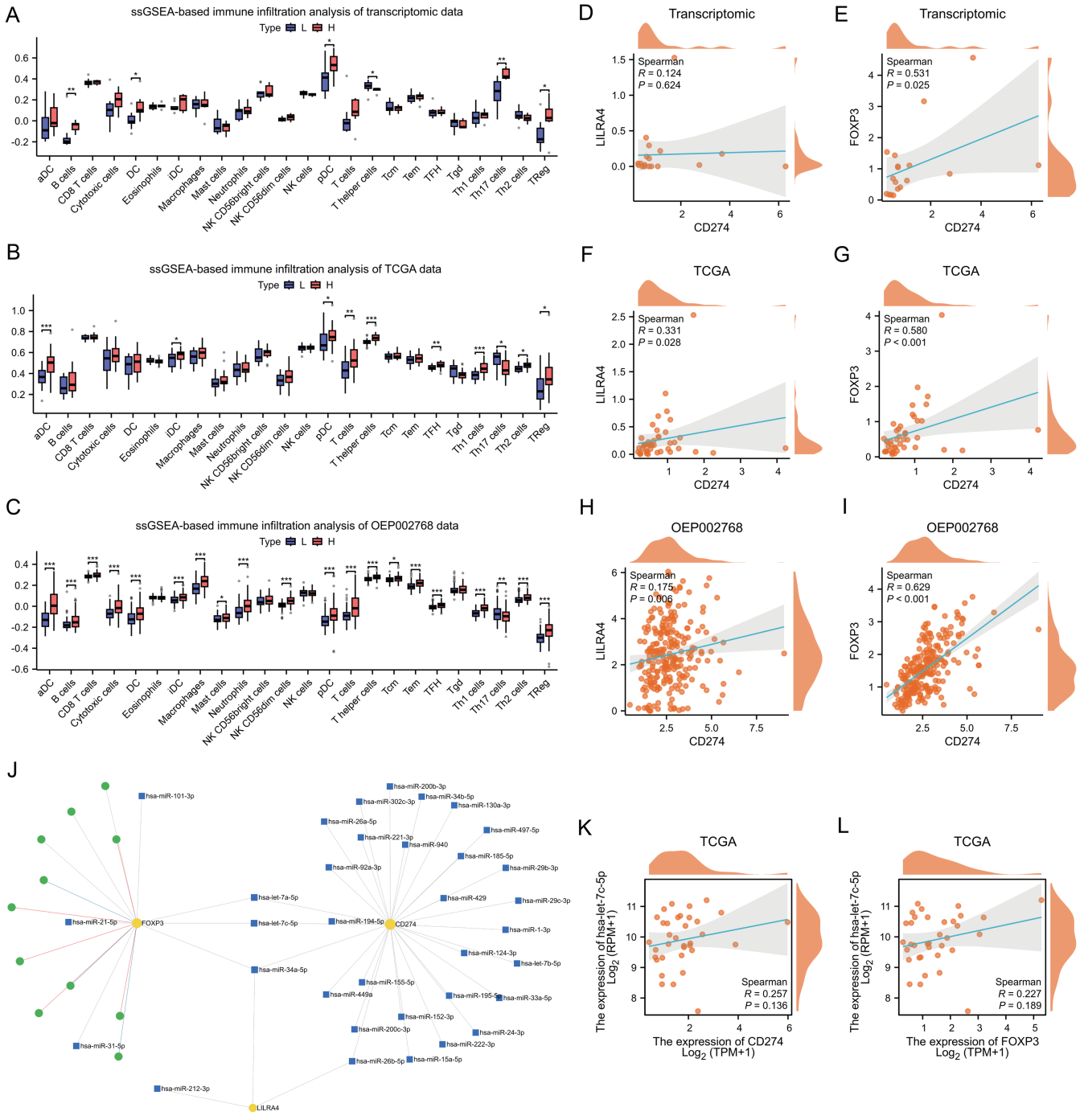

Fig. 4. Association of PD-L1 expression with immune cell infiltration profiles and a predicted miRNA-gene interaction network in ICC. (A–C) ssGSEA depicting immune cell infiltration profiles stratified by high and low CD274 (PD-L1) expression in the (A) Proteomic, (B) OEP002768, and (C) GSE107943 cohorts. (D–I) Scatter plots showing correlations between CD274 expression and key immune cell markers: (D, F, H) CD274 versus LILRA4 (a plasmacytoid dendritic cell marker) in the Proteomic, OEP002768, and GSE107943 datasets, respectively; (E, G, I) CD274 versus FOXP3 (a regulatory T cell marker) in the same respective datasets. (J) Predicted miRNA-gene interaction network for CD274, LILRA4, and FOXP3, as generated by miRNET. (K–L) Correlation analysis in the TCGA-CHOL cohort between the expression of hsa-let-7c-5p and (K) CD274, and (L) FOXP3, using integrated RNA-seq and miRNA-seq data. ICC, intrahepatic cholangiocarcinoma; ssGSEA, Single-sample Gene Set Enrichment Analysis; TCGA-CHOL, The Cancer Genome Atlas Cholangiocarcinoma.

To substantiate these findings at the marker gene level, we examined the correlations between CD274 and specific cell markers: LILRA4 for pDCs and FOXP3 for Tregs. Scatter plot analysis across all three cohorts confirmed significant positive correlations between CD274 and both immune markers (Fig. 4D–I). Strikingly, the correlation coefficients between CD274 and FOXP3 (Tregs) were consistently stronger than those between CD274 and LILRA4 (pDCs) in every dataset

analyzed, suggesting a potentially more robust biological interaction with the Treg population.

We next sought to explore the potential regulatory mechanisms underpinning these correlations. Using the miRNET platform to predict miRNA-mediated interactions, we constructed a network linking CD274, LILRA4, and FOXP3. The in-silico prediction revealed that CD274 and FOXP3 shared three common putative regulatory miRNAs, whereas CD274 and LILRA4 shared only two (Fig. 4J). This greater complexity in the potential co-regulation between CD274 and FOXP3 further supported our correlation data and led us to focus subsequent mechanistic investigations on the Treg axis.

Among the three miRNAs predicted to interact with both CD274 and FOXP3, we validated their associations using integrated RNA-seq and miRNA-seq data from the TCGA-CHOL cohort. This analysis identified hsa-let-7c-5p as a miRNA of significant interest, as its expression showed statistically significant positive correlations with both CD274 (Fig. 4K) and FOXP3 (Fig. 4L). This result nominates hsa-let-7c-5p as a potential upstream regulator coordinating the expression of PD-L1 and FOXP3 in ICC, thereby contributing to the immunosuppressive Treg-enriched microenvironment.

Single-cell transcriptomics reveals co-enrichment of TACC3 and CD274 in malignant epithelial cells

To delineate the expression dynamics of TACC3, CD274, and FOXP3 at single-cell resolution, we integrated scRNA-seq data from public datasets (GSE181878, GSE138709, GSE151530), encompassing 18 ICC tumors and 4 paracancerous tissues. Unsupervised clustering of the integrated dataset identified 22 distinct cell clusters (Fig. 5A). Batch effect correction using Harmony demonstrated successful integration across samples (Fig. 5B). These clusters were subsequently annotated into 11 major cell types through a combination of the SingleR tool and manual assessment of canonical marker genes (Fig. 5C).

Interrogation of gene expression patterns revealed that TACC3 was predominantly expressed in Proliferating cells, T cells, and Epithelial cells. CD274 was most abundant in Proliferating cells, Monocytes/Macrophages, and T cells, while FOXP3 was primarily restricted to T cells, Proliferating cells, and NK cells (Fig. 5D and E).

Given the central role of epithelial cells in ICC pathogenesis and our prior findings, we performed a focused analysis on this compartment. Re-clustering of epithelial cells yielded 19 subclusters, which we categorized into three distinct states: Intermediate, Malignant, and Normal/Benign (Fig. 5F and G). Strikingly, analysis of our key genes within these epithelial subpopulations showed that TACC3 expression was substantially higher in both Malignant and Intermediate cells compared to Normal/Benign cells (Fig. 5H and I). This observation confirms, at a cellular level, the tumor-specific upregulation of TACC3 previously identified in bulk tissue analyses. Similarly, the combined expression of CD274 in Malignant and Intermediate cells exceeded that in Normal/Benign cells, indicating its specific enrichment in neoplastic epithelial contexts. In contrast, FOXP3 expression was highest in Normal/Benign epithelial cells, suggesting that the functional interaction between TACC3 and CD274 is more prominent within the malignant epithelial compartment.

This cell state-specific co-enrichment was further corroborated at the sample level. For instance, in samples T2, T5, and T6, high levels of both TACC3 and CD274 were observed concurrently, whereas FOXP3 co-expression was limited (Fig. 5J), reinforcing the notion of a preferential interaction between TACC3 and CD274 in malignant cells.

To mechanistically link these findings, we stratified the malignant epithelial cells based on TACC3 expression. This analysis revealed that STAT3 expression was significantly elevated in the TACC3-high group compared to the TACC3-low group (Fig. 5K). This result provides compelling cellular evidence that the regulation of CD274 by TACC3 is likely mediated through STAT3 activation, rather than via a direct mechanism.

Single-cell profiling of the T-cell compartment reveals a distinct co-expression pattern of CD274 and FOXP3 in Tregs

To gain deeper insight into the immune-regulatory roles of our candidate genes within the adaptive immune compartment, we performed a focused analysis on T cells. After subsetting and re-clustering T cells from our integrated single-cell dataset, we identified 23 transcriptionally distinct T-cell subclusters (Fig. 6A). These subclusters were robustly annotated into six major functional subsets, including CD4 Effector cells, CD4 Memory cells, CD8 Effector cells, CD8 Naive cells, Proliferating T cells, and Treg cells (Fig. 6B). The refined T-cell subset information was then integrated back into the overall cellular atlas for context (Fig. 6C).

Examination of gene expression patterns within the T-cell compartment revealed a distinct cellular distribution for each molecule. As expected, FOXP3, a canonical lineage-defining transcription factor, was exclusively and highly expressed in the Treg subset (Fig. 6D and E). Intriguingly, CD274 (PD-L1) was also most abundantly expressed in Tregs, significantly higher than in other T-cell subsets. In stark contrast, TACC3 expression was relatively low across all T-cell subsets, including Tregs (Fig. 6D and E). This expression pattern suggests that within the T-cell compartment, and specifically in Tregs, the functional interaction is primarily between CD274 and FOXP3, with TACC3 likely playing a minimal direct role.

This finding was further corroborated by a heatmap visualization of gene expression across all T-cell subsets, which clearly confirmed the specific and concurrent enrichment of CD274 and FOXP3 in Tregs, while TACC3 expression remained low (Fig. 6F). The spatial distribution of these genes within the Treg subset itself was visually confirmed via UMAP projection (Fig. 6G).

To quantitatively assess the relationship between these genes specifically within Tregs, we performed a correlation analysis. The resulting correlation heatmap demonstrated a positive expression relationship between CD274 and FOXP3 across individual Treg cells (Fig. 6H). This observed co-variation strengthens the hypothesis that PD-L1 and FOXP3 are co-regulated and may function synergistically within the Treg population to mediate immunosuppressive effects in the ICC microenvironment.

Cell-cell communication and pseudotime trajectory analyses support a functional TACC3/CD274/FOXP3 axis

Given our findings that the TACC3/CD274 interaction is prominent in malignant epithelial cells while the CD274/FOXP3 interaction dominates in Tregs, we sought to investigate potential intercellular crosstalk along this axis. We first performed a comprehensive cell-cell communication analysis across all major cell types in the TME. The assessment of the number and strength of inferred interactions revealed significant communication potential between malignant epithelial cells and Tregs (Fig. 7A and B).

A detailed analysis of ligand-receptor pairs identified specific molecular pathways facilitating this bidirectional crosstalk. Tregs were predicted to send signals to malignant cells

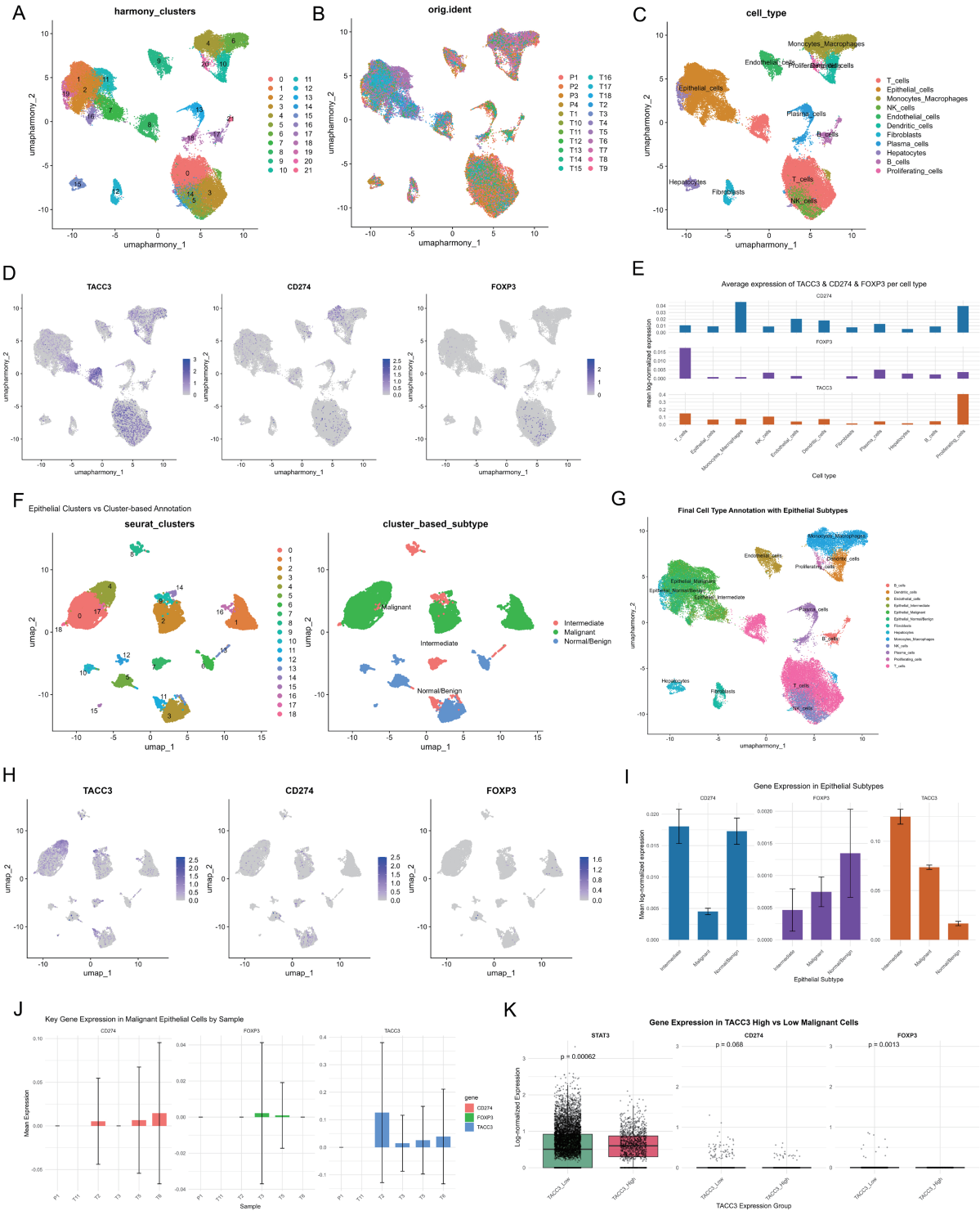

Fig. 5. Single-cell resolution of TACC3, PD-L1, and FOXP3 expression in the ICC tumor microenvironment. (A) UMAP projection of integrated scRNA-seq data from GSE181878, GSE138709, and GSE151530 (18 tumors, 4 paracancerous tissues), clustered into 22 distinct populations. (B) UMAP plot colored by sample origin. (C) UMAP plot showing preliminary cell type annotations. (D) UMAP visualizations depicting the expression distribution of TACC3, CD274 (PD-L1), and FOXP3 across all cells. (E) Bar plot showing the proportion of TACC3, CD274, and FOXP3 expression across different preliminary cell types. (F) Re-clustering of epithelial cells into 19 subclusters, annotated as Intermediate, Malignant, and Normal/Benign subtypes. (G) Final cell type annotations after integrating the refined epithelial subclasses. (H) UMAP visualization of TACC3, CD274, and FOXP3 expression specifically within the epithelial cell compartment. (I) Bar plot quantifying the expression levels of TACC3, CD274, and FOXP3 across the three epithelial subtypes. (J) Bar plot displaying the aggregate expression of TACC3, CD274, and FOXP3 across individual samples. (K) Box plots comparing the expression of STAT3, CD274, and FOXP3 in epithelial cells stratified by high- versus low-TACC3 expression. ICC, intrahepatic cholangiocarcinoma; UMAP, Uniform Manifold Approximation and Projection.

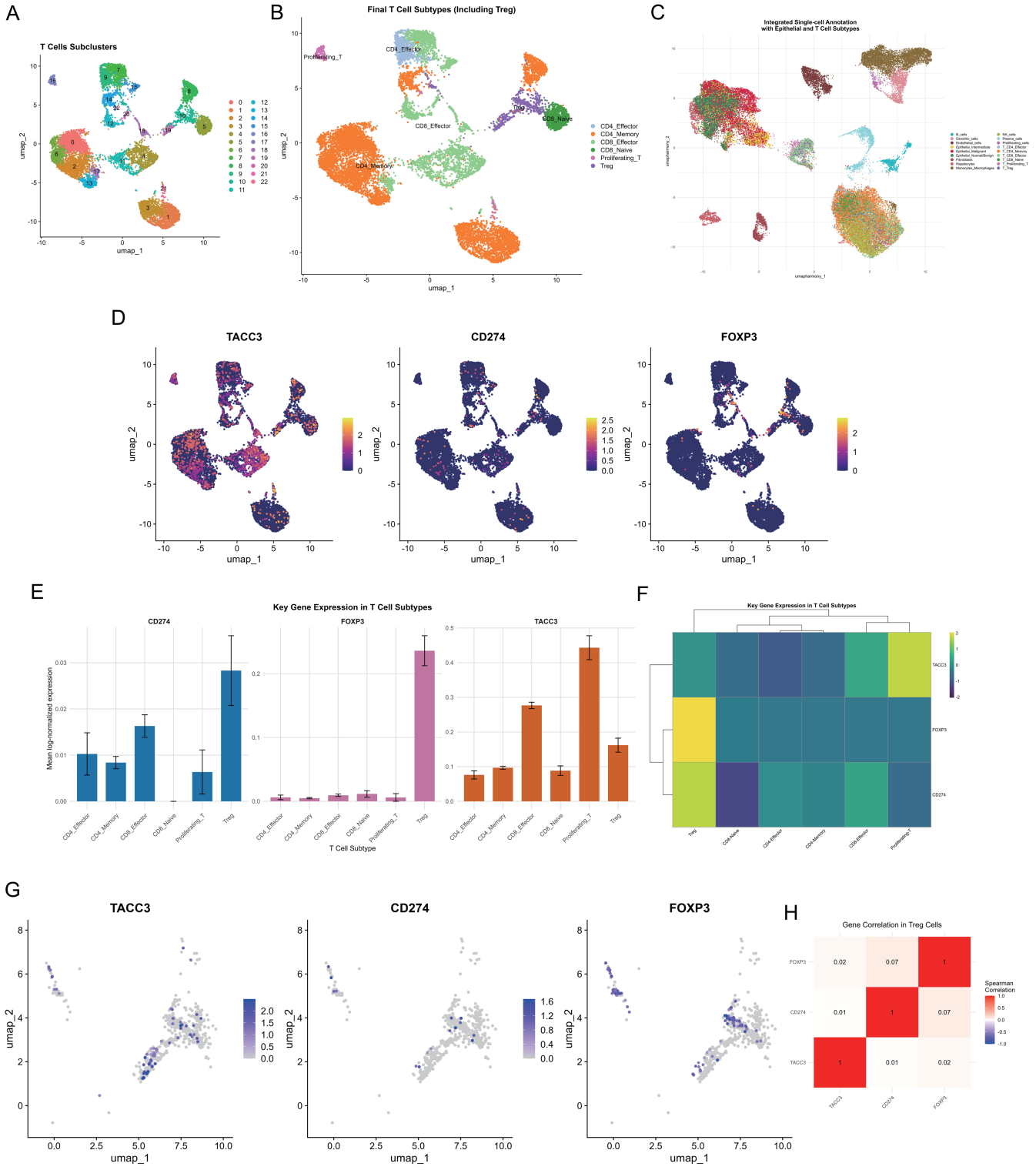

Fig. 6. Single-cell dissection of TACC3, CD274, and FOXP3 expression within the T-cell compartment of ICC. (A) UMAP visualization of T cells re-clustered into 23 distinct subpopulations. (B) Annotation of the 23 T-cell subclusters into 6 major functional subsets. (C) UMAP projection of the overall cellular landscape, with T cells highlighted according to their refined subsets. (D) UMAP plots showing the expression distribution of TACC3, CD274 (PD-L1), and FOXP3 across all T cells. (E) Bar plot quantifying the expression levels of TACC3, CD274, and FOXP3 across the defined T-cell subsets. (F) Heatmap depicting the co-expression patterns of TACC3, CD274, and FOXP3 specifically within all T cells. (G) UMAP visualization highlighting the expression of TACC3, CD274, and FOXP3 within the Treg subset. (H) Correlation heatmap analyzing the pairwise expression relationships between TACC3, CD274, and FOXP3 across individual Treg cells. ICC, intrahepatic cholangiocarcinoma; UMAP, Uniform Manifold Approximation and Projection; Treg, Regulatory T cells.

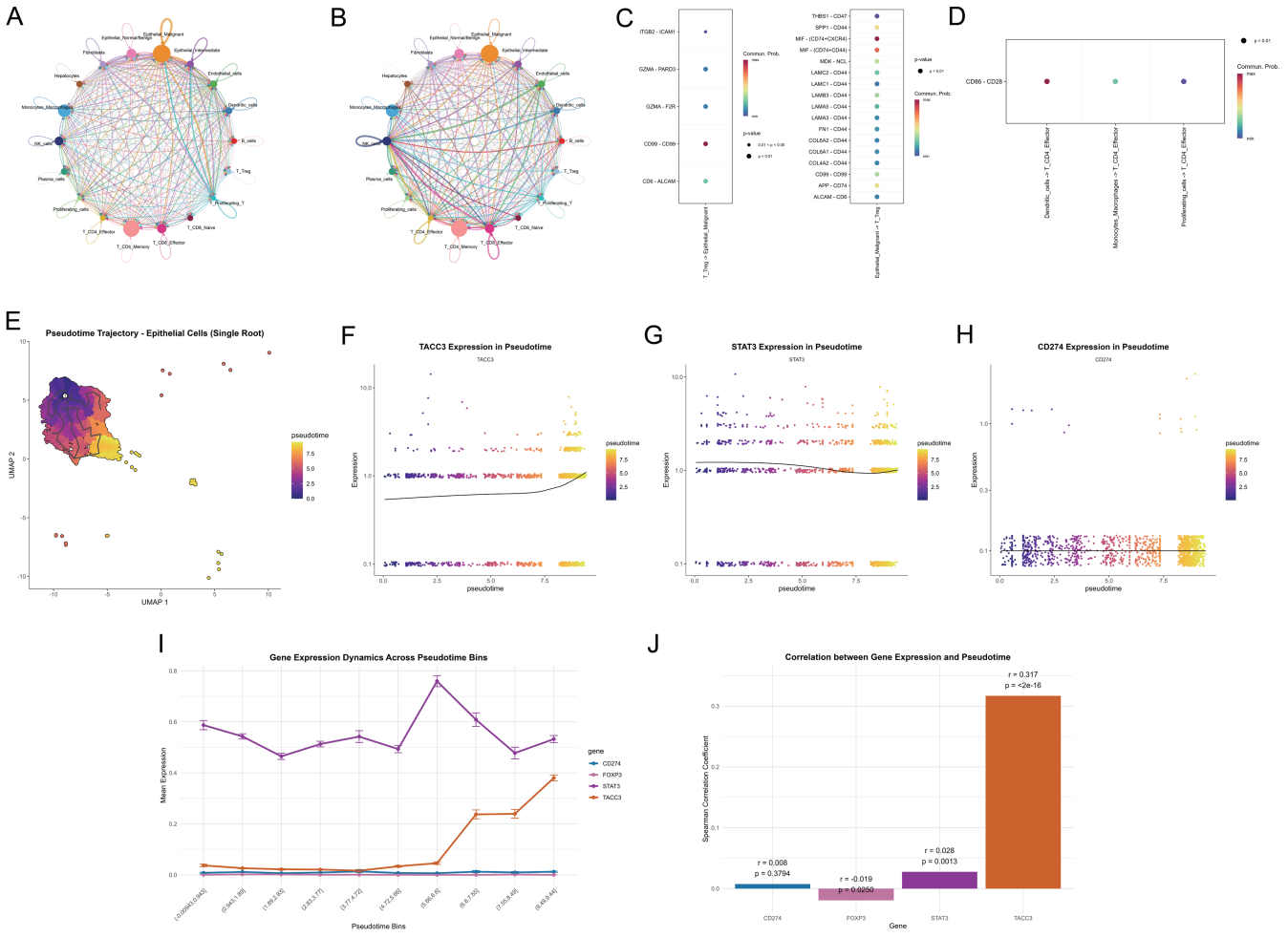

Fig. 7. Cell-cell communication and pseudotemporal dynamics of key genes in the ICC microenvironment. (A) Chord plot showing the number of inferred interactions (outgoing and incoming) for each cell type. (B) Chord plot summarizing the overall interaction strength (outgoing and incoming) for each cell type. (C) Bubble plot detailing the significant ligand-receptor interactions between Malignant epithelial cells and Tregs. (D) Bubble plot visualizing the specific CD86-CD28 interaction network across all cell types. (E) Pseudotime trajectory analysis of epithelial cells, depicting the transition from a Normal/Benign to a Malignant state. (F–H) Expression dynamics of (F) TACC3, (G) STAT3, and (H) CD274 along the pseudotime trajectory. (I) Smoothed expression patterns of TACC3, STAT3, CD274, and FOXP3 across distinct pseudotime intervals. (J) Correlation analysis between the expression of TACC3, STAT3, CD274, FOXP3, and the pseudotime ordering. ICC, intrahepatic cholangiocarcinoma; Treg, Regulatory T cells.

via pairs such as ITGB2-ICAM1, GZMA-PARD3, and CD99-CD99. Conversely, malignant cells communicated with Tregs through pairs including THBS1-CD47, SPP1-CD44, and notably, the CD99-CD99 homotypic interaction, which emerged as a key player in this reciprocal dialogue (Fig. 7C). Furthermore, analysis of the well-characterized co-stimulatory pathway CD86-CD28 showed its broad involvement in intercellular signaling (Fig. 7D), suggesting a context where PD-L1 (CD274) could potentially exert its known immunomodulatory functions.[26,27]

To delineate the dynamics of our candidate genes during tumorigenesis, we constructed a pseudotime trajectory modeling the transition from Normal/Benign to Malignant epithelial states (Fig. 7E). Analysis of gene expression along this trajectory revealed that TACC3 expression increased progressively during the malignant transformation, underscoring its pro-tumorigenic role (Fig. 7F). Similarly, STAT3 expression was upregulated in the mid-to-late phases of tumor progression (Fig. 7G). In contrast, the expression level of CD274 remained relatively stable and showed no significant change along the pseudotime continuum (Fig. 7H).

The expression dynamics of TACC3, STAT3, CD274, and FOXP3 across defined pseudotime intervals were further visualized, corroborating these trends (Fig. 7I). Finally, correlation analysis with pseudotime ordering quantitatively confirmed the strong positive correlation of TACC3 and, to a lesser extent, STAT3 with the malignant transition. In contrast, CD274 and FOXP3 expression showed no significant correlation with pseudotime progression (Fig. 7J). This indicates that while TACC3 and its downstream effector STAT3 are intrinsically linked to the process of malignant transformation, the expression of CD274 and FOXP3 in this context is likely regulated by other microenvironmental factors rather than being a direct consequence of the epithelial transformation process itself.

Experimental validation confirms TACC3 promotes malignant phenotypes and regulates PD-L1 via STAT3 and AKT signaling

To experimentally validate our multi-omics and bioinformat-

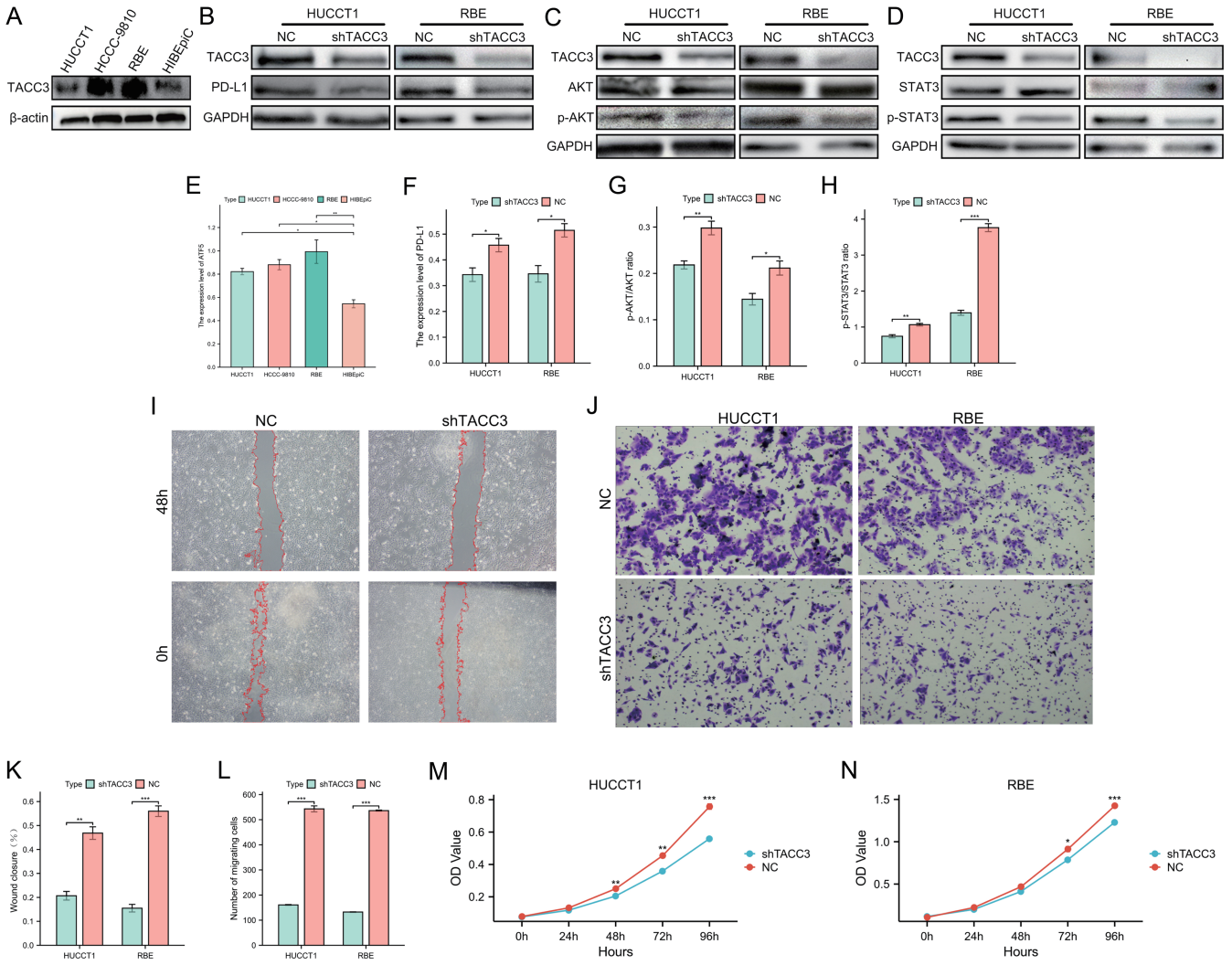

Fig. 8. Analysis of TACC3 knockdown on protein expression and malignant phenotypes in ICC cell lines. (A–H) Western blot analysis. (A, E) TACC3 protein expression in ICC cell lines (HUCCT1, HCCC9810, RBE) and human intrahepatic biliary epithelial cell line HIBEpiC. (B, F) PD-L1 protein expression in TACC3 knockdown and control cells. (C, G) Ratio of p-AKT to total AKT in TACC3 knockdown and control cells. (D, H) Ratio of p-STAT3 to total STAT3 in TACC3 knockdown and control cells. (I–N) Functional assays. (I, K) Wound healing assay of TACC3 knockdown and control cells. (J, L) Transwell migration assay of TACC3 knockdown and control cells. (M, N) CCK-8 proliferation assay of TACC3 knockdown and control cells. ICC, intrahepatic cholangiocarcinoma. $^{*}P < 0.05$, $^{**}P < 0.01$, $^{***}P < 0.001$.

ic findings, we performed a series of *in vitro* functional and molecular assays. Western blot analysis first confirmed that TACC3 protein expression was markedly elevated in three ICC cell lines (HUCCT1, HCCC9810, RBE) compared to a normal human intrahepatic biliary epithelial cell line HIBEpiC (Fig. 8A and E), corroborating its tumor-specific expression profile.

We next investigated the functional consequences of TACC3 knockdown. Silencing TACC3 led to a substantial reduction in PD-L1 protein levels (Fig. 8B and F), providing direct experimental evidence that TACC3 acts as a positive regulator of PD-L1 expression in ICC cells. To elucidate the potential signaling mechanisms downstream of TACC3, we examined the activation status of the STAT3 and AKT pathways, both of which are known upstream regulators of PD-L1. Notably, TACC3 knockdown significantly reduced the phosphorylation levels of both STAT3 (p-STAT3/STAT3 ratio) and AKT (p-AKT/AKT ratio) (Fig. 8C, D, G, and H), indicating that TACC3 modulates PD-L1, at least in part, through the activation of these key oncogenic signaling pathways.

Given the critical role of STAT3 and AKT in promoting tumor progression, we assessed the impact of TACC3 on core malignant phenotypes. Wound healing assays demonstrated that TACC3 knockdown significantly impaired cell migration, as evidenced by a decreased wound closure percentage (Fig. 8I and K). This finding was further supported by Transwell migration assays, which showed a pronounced reduction in the number of migrated cells upon TACC3 depletion (Fig. 8J and L). Furthermore, CCK-8 proliferation assays revealed that TACC3 knockdown resulted in a significant decrease in cell viability and proliferation (Fig. 8M and N).

Collectively, these functional assays demonstrate that TACC3 is essential for maintaining the migratory and proliferative capacity of ICC cells *in vitro*.

Spatial protein co-expression and clinical correlation of the TACC3/CD274/FOXP3 axis in ICC tissues

To spatially resolve the protein expression and interaction of

the TACC3/CD274/FOXP3 axis within the tissue architecture of ICC, we performed mIF staining on a TMA. Representative mIF images revealed distinct subcellular localizations: TACC3 was expressed in the cytoplasm/nucleus of tumor cells, CD274 was present on the membrane and in the cytoplasm, and FOXP3 was strictly nuclear within Treg cells (Fig. 9A). Critically, the co-localization analysis demonstrated TACC3+CD274+ signal in tumor cells (indicating their interaction in the malignant compartment) and FOXP3+CD274+ signal in Treg cells (indicating their interaction within the immune compartment), visually confirming the cell-type-specific interactions predicted by our prior analyses (Fig. 9A).

Quantitative analysis of the mIF staining using QuPath further validated our findings. The expression levels of TACC3, CD274, and FOXP3 were all significantly higher in tumor (T) tissues compared to matched peritumoral (P) tissues (Fig. 9B). Furthermore, samples classified as having high CD274 expression concurrently exhibited elevated levels of both TACC3 and FOXP3 (Fig. 9C). Correlation analysis of the protein expression data reinforced these relationships, revealing a significant positive correlation between TACC3 and CD274, and a separate significant positive correlation between CD274 and FOXP3. However, no direct correlation was observed between TACC3 and FOXP3 (Fig. 9D), solidifying the model that CD274 serves as the central link between the malignant (TACC3) and immune (FOXP3) components.

To establish the clinical relevance of our findings, we correlated TACC3 expression with patient outcomes and clinicopathological features (Supplementary Table 1). Kaplan-Meier analysis demonstrated that high TACC3 protein expression was significantly associated with a shorter progression-free survival (Fig. 9E). Moreover, elevated TACC3 expression was significantly correlated with aggressive disease characteristics, including advanced T stage, lower serum albumin levels, and the presence of microvascular invasion (Fig. 9F).

Collectively, these results from clinically annotated tissues provide strong clinical evidence that the TACC3/CD274/FOXP3 axis is operational in ICC, is driven by tumor cell-intrinsic TACC3 expression, shapes an immunosuppressive microenvironment, and ultimately contributes to tumor progression and poor clinical outcomes.

Discussion

Immunosuppression is a defining feature of the ICC TME and a major contributor to the limited efficacy of immunotherapy in this disease. Recent studies have shown that immune checkpoint inhibitors targeting the PD-1/PD-L1 axis have had limited success in ICC, with a significant proportion of patients deriving little benefit.[28,29] This underscores the urgent need to identify the upstream molecular drivers that establish and maintain this immunosuppressive niche.[30] Our multi-omics investigation, which spans transcriptomic, proteomic, and single-cell analyses, identifies TACC3 as a critical regulator of this process. By delineating a novel signaling axis wherein TACC3 activates STAT3, leading to the transcriptional upregulation of PD-L1 on tumor cells, we provide a molecular basis for the frequently observed immunosuppressive TME in ICC, positioning TACC3 as a potential master regulator of this process.

The role of TACC3 in cancer is highly context-dependent. While TACC3 has been well-known for its role in regulating mitotic spindle stability and cell cycle progression,[31] its involvement in immune modulation, particularly in ICC, remains largely unexplored. Our findings significantly expand the functional repertoire of TACC3, positioning it as a critical link between tumor cell-intrinsic signaling and extrinsic immune evasion. Previous studies have demonstrated the importance of STAT3 in immune evasion in various cancers, including ICC, where it has been shown to drive the expression of PD-L1, a key immunosuppressive marker.[32] The consistent correlation between TACC3 and PD-L1 expression across our datasets, coupled with direct experimental validation, strongly supports a causal relationship. This is further reinforced by our observation that TACC3 expression in malignant epithelial cells is positively correlated with STAT3 activation, both *in vitro* and in clinical samples.

A particularly important finding of our study, when viewed in the context of recent literature, concerns the multifaceted role of the TACC3-STAT3-PD-L1 axis in remodeling the immune landscape of ICC. Our data demonstrate that this axis not only upregulates PD-L1 on tumor cells but is also associated with a Treg-rich immunosuppressive contexture. This finding aligns with and extends the growing understanding of immune cell interplay in ICC, which has been increasingly recognized as a critical component of tumor progression.[33] For instance, a recent study identified two distinct immune infiltration patterns in ICC—macrophage-dominated and plasma cell-dominated—with the macrophage-dominated subtype, characterized by MARCO+ tumor-associated macrophages, correlating with poor prognosis and an immunosuppressive TME.[34] This underscores the critical influence of specific immune cell subsets and their spatial organization within the TME. Our findings suggest that the TACC3-STAT3-PD-L1 axis contributes to the recruitment and function of immunosuppressive immune cells, particularly Tregs, which further corroborates the findings of other studies highlighting the role of Tregs in fostering an immunosuppressive environment in cancer.[35]

The immunosuppressive functions of PD-L1 itself are now known to be more complex than just surface expression on tumor cells. A groundbreaking study revealed that Munc13-4 can regulate the sorting and secretion of PD-L1 via exosomes, mediating systemic immune suppression.[36] This mechanism allows tumor cells to exert immunosuppressive effects both locally and remotely, potentially contributing to therapy resistance. This supports our model, in which the TACC3-STAT3-PD-L1 axis acts as a linchpin in connecting tumor-intrinsic signaling with the recruitment and reinforcement of multiple immunosuppressive components, including Tregs and possibly other immune cells, sustaining an immunosuppressive niche.

Our findings are also consistent with studies in other cancers, such as hepatocellular carcinoma, where TACC3 has been implicated in mediating immunosuppression by reprogramming polyunsaturated fatty acid metabolism, impairing CD8+ T cell cytotoxicity.[37] This broadens the potential therapeutic implications of targeting TACC3 in a variety of malignancies. Notably, our single-cell RNA-seq and mIF data further validate the co-enrichment of PD-L1 and FOXP3 in Tregs and highlight the robust cellular crosstalk between malignant cells and Tregs, such as via CD99-CD99 interactions, providing further insights into how TACC3 may regulate immune suppression.

These findings carry direct clinical translational value: TACC3 may serve as a predictive biomarker for stratifying ICC patients who could benefit from immunotherapy, aligning with emerging gene-based stratification strategies in hepatobiliary malignancies; combining TACC3-targeted agents (under preclinical development) with anti-PD-L1 inhibitors may enhance efficacy by reversing STAT3-mediated immunosuppression, as supported by similar combinatorial approaches validated in ICC.[38,39]

Several limitations of our study must be acknowledged.

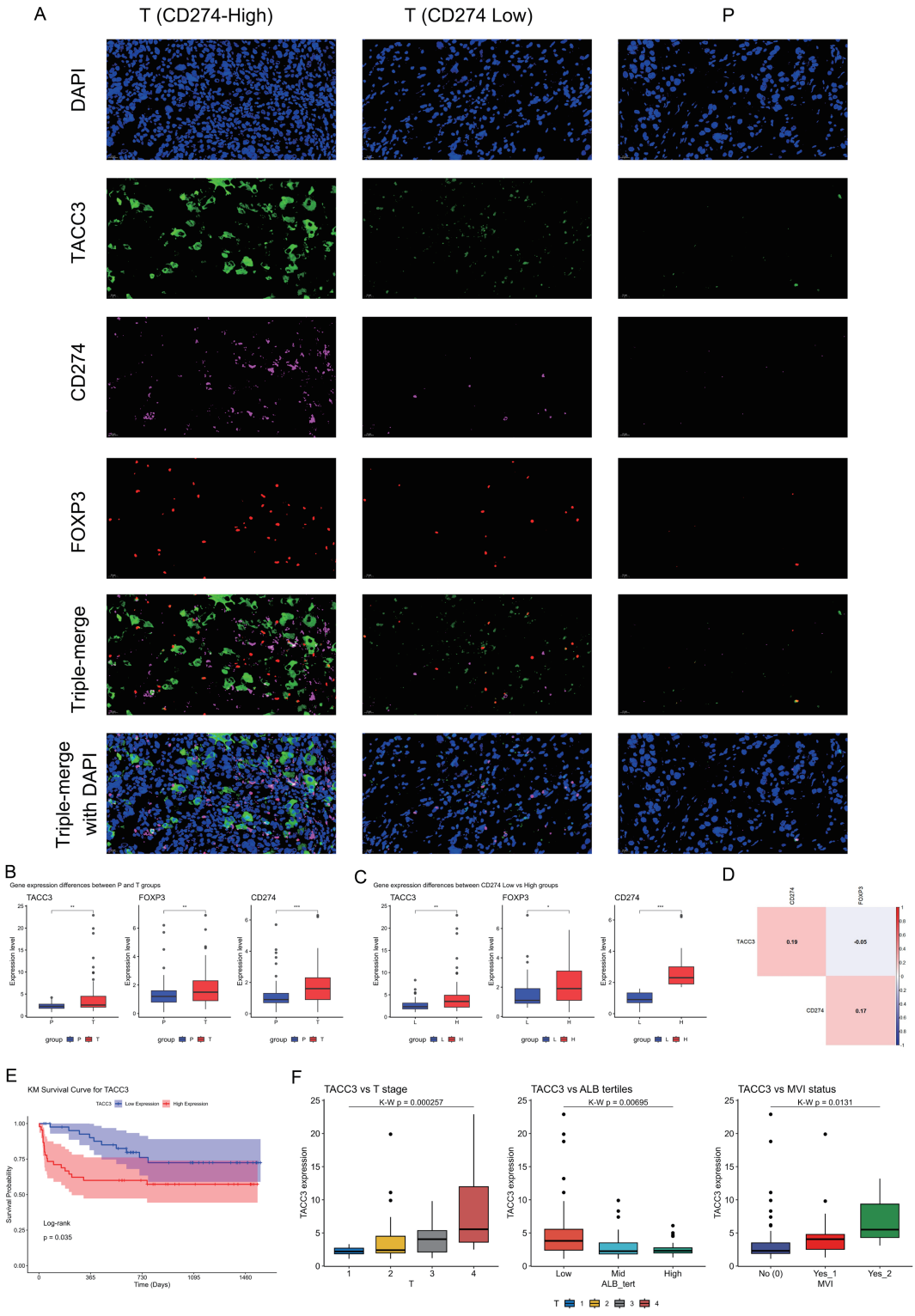

Fig. 9. TACC3, CD274, and FOXP3 protein co-expression and their clinical relevance in ICC. (A) Representative multiplex immunofluorescence images from a TMA showing the subcellular localization of TACC3 (cytoplasmic/nuclear), CD274 (membrane/cytoplasmic), and FOXP3 (nuclear) in ICC and paired peritumoral tissues. (B) Quantitative analysis of multiplex immunofluorescence staining showing the expression levels of TACC3, CD274, and FOXP3 in T tissues compared to P tissues. (C) Box plots comparing the expression levels of TACC3 and FOXP3 between samples stratified by high and low CD274 expression. (D) Correlation heatmap displaying the pairwise Pearson correlation coefficients between TACC3, CD274, and FOXP3 expression. (E) Kaplan-Meier curve comparing PFS between patients with high and low TACC3 expression. (F) Comparison of TACC3 expression levels across different T stages, ALB groups, and MVI status. ICC, intrahepatic cholangiocarcinoma; TMA, tissue microarray; T issues, tumor issues; P issues, peritumoral issues; PFS, progression-free survival; ALB, albumin; MVI, microvascular invasion. *P < 0.05, **P < 0.01, ***P < 0.001.

First, while our multi-omics cohorts are well-characterized, the sample size for the proteomic discovery phase is relatively small, which limits the statistical power and generalizability of our findings. Larger prospective cohorts are needed to validate the prognostic value of TACC3 in ICC. Second, the precise biochemical mechanism by which TACC3 activates the STAT3 and AKT pathways requires further elucidation. It remains to be determined whether this is a direct effect or mediated through interactions with upstream regulators. Finally, the *in vivo* role of TACC3 in shaping the TME and its potential as a therapeutic target warrants further investigation in immunocompetent animal models of ICC.

Conclusions

Our work unveils a novel oncogenic-immune regulatory pathway in ICC, driven by TACC3. We establish that TACC3 promotes tumor progression not only by enhancing cell proliferation and migration but also by activating STAT3 to upregulate PD-L1, thereby sculpting an immunosuppressive TME characterized by Treg infiltration. These findings provide a crucial mechanistic understanding of immune evasion in ICC and position TACC3 as a promising and previously unexplored therapeutic target. Combinatorial strategies targeting TACC3, along with immune checkpoints, may represent a viable approach to reverse immunosuppression and improve outcomes for patients with this lethal malignancy.

Acknowledgments

We gratefully acknowledge all participants of this study for their contributions.

Funding

This study was funded by the National Natural Science Foundation of China (No. 82170666 and 82572988).

Conflict of interest

RL has been an Editorial Board Member of *Journal of Clinical and Translational Hepatology* since 2022. The other authors have no conflict of interests related to this publication.

Author contributions

Study conception and design (RL, XL), material preparation, data collection and analysis (HW, HChen, HCui, YY, RX), first draft of the manuscript (ZX, ZZ), analysis and revision of the manuscript (RL). All authors have read and approved the final manuscript.

Ethical statement

This study was approved by the Ethics Committee of the First Affiliated Hospital of Chongqing Medical University (Approval No. 2024-180-01). All participants provided informed consent before participation. The study was conducted in accordance with the Declaration of Helsinki (as revised in 2024), and all clinical procedures were performed following the ethical guidelines for human research.

Data sharing statement

The datasets and materials supporting our findings in the current study are available from the corresponding authors upon reasonable request.

References

[1] Chang YJ, Chang YJ, Chen LJ. Prognostic factors in patients with intrahepatic cholangiocarcinoma. Sci Rep 2024;14(1):19084. doi:10.1038/s41598-024-70124-z, PMID:39154139.
[2] Deng L, Bao W, Zhang B, Zhang S, Chen Z, Zhu X, *et al*. AZGP1 activation by lenvatinib suppresses intrahepatic cholangiocarcinoma epithelial-mesenchymal transition through the TGF-β1/Smad3 pathway. Cell Death Dis 2023;14(9):590. doi:10.1038/s41419-023-06092-5, PMID:37669935.
[3] Yu Y, You Y, Duan Y, Kang M, Zhou B, Yang J, *et al*. Multi-omics approaches for identifying the PANoptosis signature and prognostic model via a multimachine-learning computational framework for intrahepatic cholangiocarcinoma. Hepatology 2026;83(3):466–483. doi:10.1097/HEP.0000000000001352, PMID:40233411.
[4] Liu X, Yao J, Song L, Zhang S, Huang T, Li Y. Local and abscopal responses in advanced intrahepatic cholangiocarcinoma with low TMB, MSS, pMMR and negative PD-L1 expression following combined therapy of SBRT with PD-1 blockade. J Immunother Cancer 2019;7(1):204. doi:10.1186/s40425-019-0692-z, PMID:31383016.
[5] Huang S, Hua C, Ding B, Chen J, Zheng S, Ding C. Advances in improving the efficacy of anti-PD-1/PD-L1 therapy in intrahepatic cholangiocarcinoma. Crit Rev Oncol Hematol 2025;213:104784. doi:10.1016/j.critrevonc.2025.104784, PMID:40447208.
[6] Prawira A, Xu H, Mei Y, Leow WQ, Nasir NJM, Reolo MJ, *et al*. Targeting Treg-fibroblast interaction to enhance immunotherapy in steatotic liver disease-related hepatocellular carcinoma. Gut 2025;75(1):105–118. doi:10.1136/gutjnl-2025-335084, PMID:40695620.
[7] Ogunlusi O, Sarkar M, Carter K, Chakrabarti A, Boland DJ, Nguyen T, *et al*. LILRB4 regulates circadian disruption-induced mammary tumorigenesis via non-canonical WNT signaling pathway. Oncogene 2025;44(46):4491–4504. doi:10.1038/s41388-025-03597-5, PMID:41102383.
[8] Alicea Pauneto CDM, Riesenberg BP, Gandy EJ, Kennedy AS, Clutton GT, Hem JW, *et al*. Intra-tumoral hypoxia promotes CD8(+) T cell dysfunction via chronic activation of integrated stress response transcription factor ATF4. Immunity 2025;58(10):2489–2504.e8. doi:10.1016/j.immuni.2025.09.003, PMID:41005293.
[9] Li S, Lin J, Huang L, Hu S, Wang M, Sun W, *et al*. STK31 drives tumor immune evasion through STAT3-IL-6 mediated CD8(+) T cell exhaustion. Oncogene 2025;44(20):1452–1462. doi:10.1038/s41388-024-03271-2, PMID:40025230.
[10] Jia L, Wang Y, Wang CY. circFAT1 Promotes Cancer Stemness and Immune Evasion by Promoting STAT3 Activation. Adv Sci (Weinh) 2021;8(13):2003376. doi:10.1002/advs.202003376, PMID:34258151.
[11] Saatci O, Akbulut O, Cetin M, Sikirzhytski V, Uner M, Lengerli D, *et al*. Targeting TACC3 represents a novel vulnerability in highly aggressive breast cancers with centrosome amplification. Cell Death Differ 2023;30(5):1305–1319. doi:10.1038/s41418-023-01140-1, PMID:36864125.
[12] Modi A, Vai S, Caramelli D, Lari M. The Illumina Sequencing Protocol and the NovaSeq 6000 System. Methods Mol Biol 2021;2242:15–42. doi:10.1007/978-1-0716-1099-2_2, PMID:33961215.
[13] Basu A, Chiriboga L, Narula N, Zhou F, Moreira AL. Validation of PD-L1 clone 22C3 immunohistochemical stain on two Ventana DISCOVERY autostainer models: detailed protocols, test performance characteristics, and interobserver reliability analyses. J Histotechnol 2020;43(4):174–181. doi:10.1080/01478885.2020.1823105, PMID:33245263.
[14] Taxman DJ, Livingstone LR, Zhang J, Conti BJ, Iocca HA, Williams KL, *et al*. Criteria for effective design, construction, and gene knockdown by shRNA vectors. BMC Biotechnol 2006;6:7. doi:10.1186/1472-6750-6-7, PMID:16433925.
[15] Sule R, Rivera G, Gomes AV. Western blotting (immunoblotting): history, theory, uses, protocol and problems. Biotechniques 2023;75(3):99–114. doi:10.2144/btn-2022-0034, PMID:36971113.
[16] Ishiyama M, Miyazono Y, Sasamoto K, Ohkura Y, Ueno K. A highly water-soluble disulfonated tetrazolium salt as a chromogenic indicator for NADH as well as cell viability. Talanta 1997;44(7):1299–1305. doi:10.1016/s0039-9140(97)00017-9, PMID:18966866.
[17] Justus CR, Marie MA, Sanderlin EJ, Yang LV. Transwell In Vitro Cell Migration and Invasion Assays. Methods Mol Biol 2023;2644:349–359. doi:10.1007/978-1-0716-3052-5_22, PMID:37142933.
[18] Butler A, Hoffman P, Smibert P, Papalexi E, Satija R. Integrating single-cell transcriptomic data across different conditions, technologies, and species. Nat Biotechnol 2018;36(5):411–420. doi:10.1038/nbt.4096, PMID:29608179.
[19] Sun Z, Nyberg R, Wu Y, Bernard B, Redmond WL. Developing an enhanced 7-color multiplex IHC protocol to dissect immune infiltration in human cancers. PLoS One 2021;16(2):e0247238. doi:10.1371/journal.pone.0247238, PMID:33596250.
[20] Li C, Li Y, Zhang H, Zhuo Y, Zhang L, Yang L, *et al*. Xuanfei Baidu Decoction suppresses complement overactivation and ameliorates IgG immune complex-induced acute lung injury by inhibiting JAK2/STAT3/SOCS3 and NF-κB signaling pathway. Phytomedicine 2023;109:154551. doi:10.1016/j.phymed.2022.154551, PMID:36610119.
[21] Xing C, Zhuang Y, Xu TH, Feng Z, Zhou XE, Chen M, *et al*. Cryo-EM Structure of the Human Cannabinoid Receptor CB2-G(i) Signaling Complex. Cell 2020;180(4):645–654.e13. doi:10.1016/j.cell.2020.01.007, PMID:32004460.
[22] Taifour T, Attalla SS, Zuo D, Gu Y, Sanguin-Gendreau V, Proud H, *et al*. The tumor-derived cytokine Chi3l1 induces neutrophil extracellular traps that promote T cell exclusion in triple-negative breast cancer. Immunity 2023;56(12):2755–2772.e8. doi:10.1016/j.immuni.2023.11.002, PMID:38039967.

[23] Song M, Wang Y, Annex BH, Popel AS. Experimental and computational studies of IL-6 signaling in endothelial cells under hypoxia serum starvation conditions. Cytokine 2025;195:157029. doi:10.1016/j.cyto.2025.157029, PMID:40946487.
[24] Foerster EG, Mukherjee T, Cabral-Fernandes L, Rocha JDB, Girardin SE, Philpott DJ. How autophagy controls the intestinal epithelial barrier. Autophagy 2022;18(1):86–103. doi:10.1080/15548627.2021.1909406, PMID:33906557.
[25] Han H, Li Q, Wang C, Liang Z, Zhang L, Zhang S, *et al*. Hypothalamic BCL6 signaling modulates energy homeostasis and metabolism by inhibiting STAT3 transcription. J Adv Res 2026;82:953–965. doi:10.1016/j.jare.2025.07.028, PMID:40701335.
[26] Sagiv-Barfi I, Czerwinski DK, Levy S, Alam IS, Mayer AT, Gambhir SS, *et al*. Eradication of spontaneous malignancy by local immunotherapy. Sci Transl Med 2018;10(426):eaan4488. doi:10.1126/scitranslmed.aan4488, PMID:29386357.
[27] Smith-Garvin JE, Koretzky GA, Jordan MS. T cell activation. Annu Rev Immunol 2009;27:591–619. doi:10.1146/annurev.immunol.021908.132706, PMID:19132916.
[28] Yin Z, Zhang L, Li J, Tan H, Ma B. Research progress on immune checkpoint inhibitors in intrahepatic cholangiocarcinoma. Ann Med 2025;57(1):2584667. doi:10.1080/07853890.2025.2584667, PMID:41236411.
[29] Cao Y. Cancer-triggered systemic disease and therapeutic targets. Holist Integr Oncol 2024;3(1):11. doi:10.1007/s44178-024-00077-w, PMID:38482486.
[30] Zhou G, Sprengers D, Mancham S, Erkens R, Boor PPC, van Beek AA, *et al*. Reduction of immunosuppressive tumor microenvironment in cholangiocarcinoma by ex vivo targeting immune checkpoint molecules. J Hepatol 2019;71(4):753–762. doi:10.1016/j.jhep.2019.05.026, PMID:31195061.
[31] Shi S, Guo D, Ye L, Li T, Fei Q, Lin M, *et al*. Knockdown of TACC3 inhibits tumor cell proliferation and increases chemosensitivity in pancreatic cancer. Cell Death Dis 2023;14(11):778. doi:10.1038/s41419-023-06313-x, PMID:38012214.
[32] Song TL, Nairismägi ML, Laurensia Y, Lim JQ, Tan J, Li ZM, *et al*. Oncogenic activation of the STAT3 pathway drives PD-L1 expression in natural killer/T-cell lymphoma. Blood 2018;132(11):1146–1158. doi:10.1182/blood-2018-01-829424, PMID:30054295.
[33] Konishi D, Umeda Y, Yoshida K, Shigeyasu K, Yano S, Toji T, *et al*. Regulatory T cells induce a suppressive immune milieu and promote lymph node metastasis in intrahepatic cholangiocarcinoma. Br J Cancer 2022;127(4):757–765. doi:10.1038/s41416-022-01838-y, PMID:35597869.
[34] Fan G, Tao C, Li L, Xie T, Tang L, Han X, *et al*. The co-location of MARCO+ tumor-associated macrophages and CTSE+ tumor cells determined the poor prognosis in intrahepatic cholangiocarcinoma. Hepatology 2025;82(1):25–41. doi:10.1097/HEP.0000000000001138, PMID:39471066.
[35] Li C, Jiang P, Wei S, Xu X, Wang J. Regulatory T cells in tumor microenvironment: new mechanisms, potential therapeutic strategies and future prospects. Mol Cancer 2020;19(1):116. doi:10.1186/s12943-020-01234-1, PMID:32680511.
[36] Liu C, Liu D, Zheng X, Guan J, Zhou X, Zhang H, *et al*. Munc13-4 mediates tumor immune evasion by regulating the sorting and secretion of PD-L1 via exosomes. Nat Commun 2025;16(1):9080. doi:10.1038/s41467-025-64149-9, PMID:41083534.
[37] Li Y, Chen Z, Wang D, Du W, Zhu N, Shen X, *et al*. Transforming acidic coiled-coil-containing protein 3-mediated lipid metabolism reprogramming impairs CD8(+) T-cell cytotoxicity in hepatocellular carcinoma. Signal Transduct Target Ther 2025;10(1):274. doi:10.1038/s41392-025-02367-9, PMID:40866361.
[38] Gedik ME, Saatci O, Oberholtzer N, Uner M, Akbulut Caliskan O, Cetin M, *et al*. Targeting TACC3 Induces Immunogenic Cell Death and Enhances T-DM1 Response in HER2-Positive Breast Cancer. Cancer Res 2024;84(9):1475–1490. doi:10.1158/0008-5472.CAN-23-2812, PMID:38319231.
[39] Scholer AJ, Marcus RK, Garland-Kledzik M, Ghosh D, Ensenyat-Mendez M, Germany J, *et al*. Exploring the Genomic Landscape of Hepatobiliary Cancers to Establish a Novel Molecular Classification System. Cancers (Basel) 2024;16(2):325. doi:10.3390/cancers16020325, PMID:38254814.